

Wrinkling behavior of laminated steel sheets

H.S. Cheng^a, J. Cao^{a,*}, H. Yao^b, S.D. Liu^b, B. Kinsey^c

^a Department of Mechanical Engineering, Northwestern University, Evanston, IL 60208, USA

^b National Steel Corporation, USA

^c University of New Hampshire, Durham, USA

Abstract

Laminated steel sheets sandwiched with a polymer core are increasingly used for automotive applications to improve vehicle's vibration-damping performance without adding additional weight. It has been observed that the laminated sheets are prone to wrinkling during stamping processes. Due to the significant difference in material properties between the polymer core and the skin steel, FEM prediction of the occurrence, the location, and the shapes of wrinkles in the forming of laminated sheets is still a great challenge.

In this paper, the Yoshida buckling test and wedge strip test of laminated steel and its steel skins were conducted. The information of local strains, buckling heights and global wrinkling patterns were obtained in order to study the initiation condition of wrinkling and the post-buckling behavior of the sheets, and to provide verification data for numerical predictions. Rectangular panel forming tests were also conducted. The results showed that the 1.0 mm laminated sheet employed has a wrinkling tendency similar to that of its 0.5 mm skin panel and has a strain distribution similar to that of its 1.0 mm solid counterpart.

© 2004 Elsevier B.V. All rights reserved.

Keywords: Wrinkling; Laminate; Forming; Sheet metal

1. Introduction

Laminated steel sheets sandwiched with a polymer core are increasingly used for automotive application due to their superior vibration and sound damping properties [1]. Two types of laminated sheets, i.e. light weight laminated steel with a thick polymer core (SPS) and laminated vibration damping steel (LVDS) with a thin polymer adhesive core have been utilized in automotive manufacturing to reduce the weight of or improve the noise-vibration harshness (NVH) performance. In this paper, the authors concentrate on studying the wrinkling behavior of LVDS.

The behavior of laminated sheets is very different from that of homogenous steel sheets in the forming process due to the huge difference in material properties of the polymer core and the steel skins. Finite element simulation of laminated steel forming has become a great challenge. Spring elements and a Tie-Break interface have been used to model laminated structures and good correlations have been obtained between numerical and experimental results in V-bending, deep drawing and dash panel forming cases [2].

Wrinkling is one of the major defects in sheet metal forming, together with tearing, spring-back and other geometric and surface defects. Many research efforts have been dedicated to predict the occurrence, the location, and the shape of the wrinkles as evident in the review articles [3–5], which emphasized the work initiated from Hill's general theory of uniqueness and bifurcation [6]. Tomita [3] and Petryk [4] discussed the importance of material models on the prediction results. In most of the finite element analyses (FEA), accumulated computational error can be treated as an artificial imperfection in the system to initiate the wrinkling, but the necessary magnitude to initiate wrinkling is problem dependent. This nature determines the uncertainties associated with the FEA in practical applications. Wang and Cao [7] proposed a stress-based wrinkling predictor. Cao et al. [8] developed a multi-scale approach with mesh-free adaptivity [9] to simulate the wrinkling behavior of sheet metals, while using the stress-based predictor to generate the desired enrichment function. This method is now able to capture the wrinkling and post-buckling behavior in an elastic plate and wedge strip examples [10].

With all the numerical work, it is necessary to have well-controlled experiments to verify the numerical approaches. The experimental work can be divided into two categories. The first category includes simple tests of special specimens designed for simulating the basic mechanism in

* Corresponding author. Tel.: +1-847-467-1032.
E-mail address: jcao@northwestern.edu (J. Cao).

sheet metal forming. Among them, the most widely used test method to study the wrinkling phenomenon is the Yoshida buckling test [11], in which a thin square plate is stretched diagonally to study the effect of material properties on the onset of buckling and buckling height. The other category is actual forming of typical components with simple geometries such as the Swift cup test [12] and the annular plate-drawing test [13]. Compared to the tests in the first category, these tests can study the effects of more factors on wrinkling behavior, such as forming parameters and tooling geometry. Depending on the tooling geometry and binder pressure, wrinkling may occur in the flange and/or side-wall areas. However, the tooling cost of these forming tests is much higher than those of the simple tests and it is difficult to obtain real-time strain information in forming tests.

Recently, Cao et al. [14] designed a novel wedge strip test, which simulated various boundary conditions in forming processes where wrinkles would initiate. Incorporated with a state-of-the-art high resolution laser digitizer, the wedge strip test is able to capture the high resolution real-time out-of-plane deformation image of the tested sample [8]. Cheng et al. [10] used this experiment to study the buckling behavior of laminated sheets.

In this paper, a new design of the wedge strip test is introduced in Section 2 to increase the test repeatability and experimental results are presented with three different materials: 1.0 mm thick laminate sheet, 0.5 mm solid sheet and 1.0 mm solid sheet. In addition, the Yoshida buckling test and the rectangular panel forming test introduced in Sections 3 and 4, respectively, were conducted with these three materials. Finally, the conclusions were given in Section 5.

2. Wedge strip tests

2.1. Experimental set-up

The basic experimental set-up has been introduced by Cao et al. [8,14]. Fig. 1 shows an overview of the set-up. In this paper, a new fixture is designed to deform a wedge strip specimen as shown in Fig. 2. The sample sheet can slide within the well-lubricated side guide plates with a friction coefficient of less than 0.04 achieved with Teflon membranes. The gap between the two guide plates can be varied to accommodate samples with different thicknesses. Two L-shaped arms and the guide plates are all adjustable in order to set up different boundary conditions and to simulate forming processes where wrinkles would initiate. Compared with the first generation of the fixture introduced by Cao et al. [14], the enhanced version is more precise, adjustable and rigid. When the top end of the specimen is clamped and pulled upwards by the grip of a tensile test machine, compressive stress is generated in the plane of the sheet along the transverse direction perpendicular to the loading direction due to the side restrictions and specimen geometry.

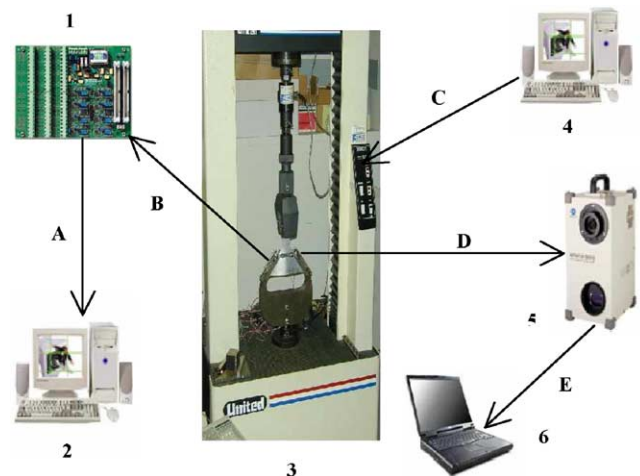


Fig. 1. Experimental set-up of the wedge strip test.

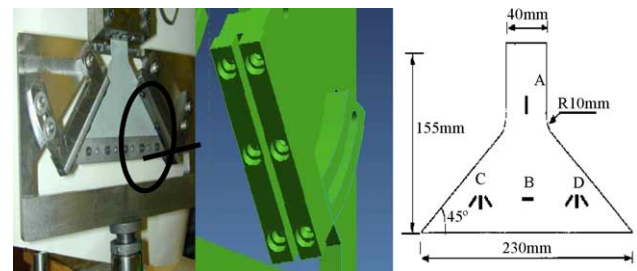


Fig. 2. Fixture and specimen.

Three materials have been tested: (1) 1.016 mm thick electro-galvanized laminated AKDQ steel (laminated); (2) 1.016 mm thick electro-galvanized AKDQ steel (1 mm solid); and (3) 0.519 mm thick electro-galvanized AKDQ steel (0.5 mm solid, which is the substrate of the laminate). The laminated sheet is made with two layers of 0.5 mm solid sheets bonded together by a thin layer of adhesive (Fig. 3). Their properties are listed in Table 1.

The tensile machine has a maximum capacity of 89 kN. The loading speed was kept at 0.25 mm/min. As shown in Fig. 2, for each test, two micro measurements MM-EA-06-125AD-120 single element strain gages are mounted at positions A and B to measure the longitudinal strain and the transverse compressive strain. Due to the possible asymmetric buckling mode, two micro-measurements MM-EA-06-125RA-120 three-element rosettes are mounted at positions C and D, respectively, to measure the in-plane strains. All gages are wired to a PC via a National

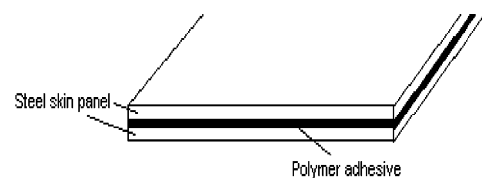


Fig. 3. The cross-section of a laminate sheet.

Table 1
Material properties of laminated and single layer sheets (from the National Steel Corporation)

Properties	Laminate	Solid (1 mm)	Solid (0.5 mm)
Yield strength (MPa)	178	148	209
Tensile strength (MPa)	284	303	318
<i>n</i> -Value	0.214	0.238	0.211
<i>K</i> -Value (MPa)	520	551	546
Thickness (mm)	1.016	1.016	0.519

Instruments NI-SC-2043-SG signal-conditioning board. The testing range of the strain gage is ±3%, along with the resolution of 0.00188%. A PC controlled Minolta VIVID-900 laser digitizer is used to measure the deformation. The resolution is 0.05 mm in the Z-depth direction and 0.175 mm in the X and Y plane.

In this wedge strip test, two different boundary conditions are investigated here:

- *Boundary condition #1 (B1)*: the bottom of the sheet is free, and two sides are restricted by the guide plates.
- *Boundary condition #2 (B2)*: the bottom of the sheet is clamped, and two sides are restricted.

2.2. Results and discussion

2.2.1. B1 condition

Under the B1 condition, a symmetrical buckling mode was observed. Fig. 4 shows the 3D deformation contour of a buckled sample from the laser digitizer. Buckling occurs at a very early stage in terms of clamp displacement, as shown in Fig. 5. The Roman number in the caption of Fig. 5 and later figures in this paper represents different experimental tests. The 0.5 mm sheets started buckling when the clamp displacement reached about 0.04 mm, then the buckling height increased steadily. The buckling initiation points for the laminate and 1 mm sheets are both at around 0.14 mm. However, the laminate sheet had a dramatic amount of increase of buckling height at the initiation point, behaving similarly to the 0.5 mm sheets. This might be due to the possible delamination in the laminate sheet at the point of buckling. The amount of 1 mm sheets showed more resistance and their buckling heights increased relatively slowly. When strains are concerned, the three materials all started to buckle at a longitudinal strain of 0.004% at point A (Fig. 2) and a compressive strain at point B of less than 0.01%.

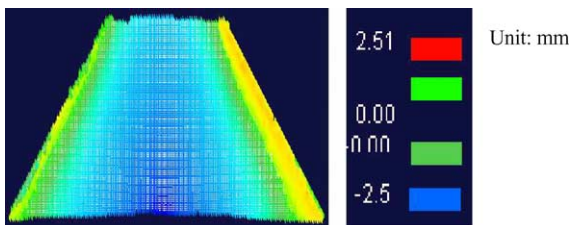


Fig. 4. Deformation contour under the B1 condition.

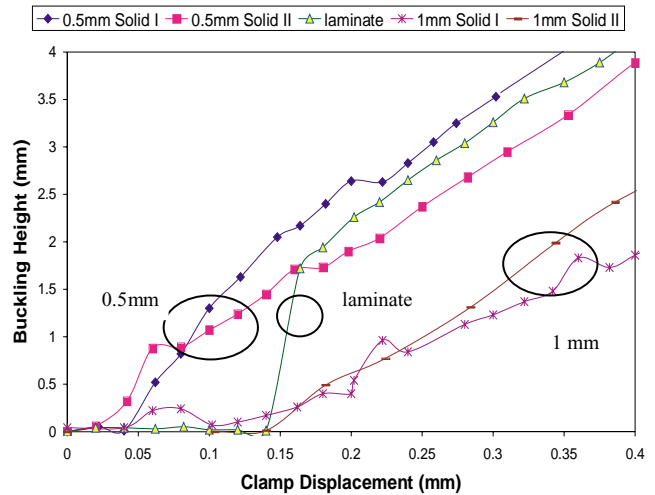


Fig. 5. Buckling height vs. clamp displacement (B1).

Figs. 5 and 6 indicate that for all the materials, buckling initiated when the sheets were still under elastic deformation. After the clamp displacement reached about 1 mm, the samples were removed from the fixture whereupon they recovered various amounts of the buckling deformation. Table 2 shows that there are large amounts of elastic buckling in the 0.5 mm solid and laminate sheets because of the thinner material, while the 1 mm solid has very little recoverable buckling.

2.2.2. B2 condition

Under the B2 boundary condition, the bottom of the sample is clamped to maintain a zero slope at all edges of the sheet. This is usually the case where sheet metal has side-wall wrinkling inside the die-opening line. Fig. 7 is the 3D deformation contours under the B2 condition. Two buckling modes were observed. The symmetrical buckling mode only occurred with 1 mm solid sheets. The asymmetrical mode occurred with all of the materials.

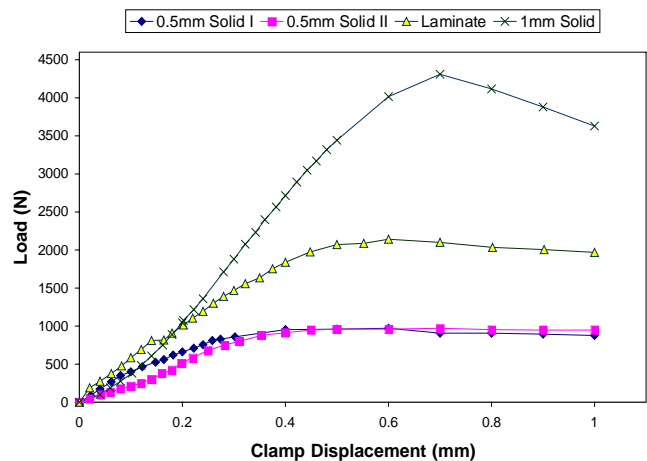


Fig. 6. Tensile load vs. clamp displacement (B1).

Table 2
Buckling recovered under the B1 condition

Materials	Clamp displacement (mm)	Buckling height (mm)	Buckling height after unloading (mm)	Recovered (%)
Solid (0.5 mm)	1.0	9.27	6.25	33
Solid (0.5 mm)	1.0	8.82	5.4	39
Laminated	1.0	9.41	5.75	39
Laminated	0.902	7.25	5.02	31
Solid (1 mm)	1	7.88	7.55	5
Solid (1 mm)	1.304	10.51	9.25	12

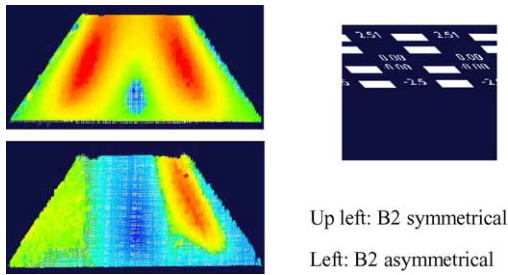


Fig. 7. The 3D deformation contours (B2).

In the asymmetrical mode, the sequence of the initiations of the two buckling modes is not obvious. Fig. 8 shows a few cases where the central buckling and side buckling were initiated simultaneously (a slope change of the buckling height with respect to either the displacement or the compressive strain), while in other cases the central buckling occurred first. It should be noticed that the two buckling modes have reverse directions. Despite the order of the initiations, the side buckling always dominated at the end. Coupled with

the side buckling, the central buckling started to fade when the sample was pulled to a certain amount, depending on the materials being tested.

In the case where the central buckling was initiated earlier than the side buckling, the transition pattern is similar to the 0.76 mm thick HSG25S steel [8]. It can be believed that for buckling mode transition to occur, the system passes at least two bifurcation points under the test. At the first bifurcation point, it switches from the ‘flat branch’ to half-wave branch. Similarly at the second point, the half-wave becomes unstable and the system transfers to the stable one-wave mode. Locally, large effective regions are the main reason to cause the instability in the side area [14]. The inevitable imperfection of the specimen and the fixture introduced asymmetry to the system that triggers the side buckling mode. The 0.5 mm solid and laminate sheets are more sensitive to the imperfection.

Fig. 9 indicates that the 1 mm solid sheet has a much higher buckling resistance than the other two materials, while the 0.5 mm solid and laminate sheets have similar resistance. For 1 mm sheets, the initiation points lie between

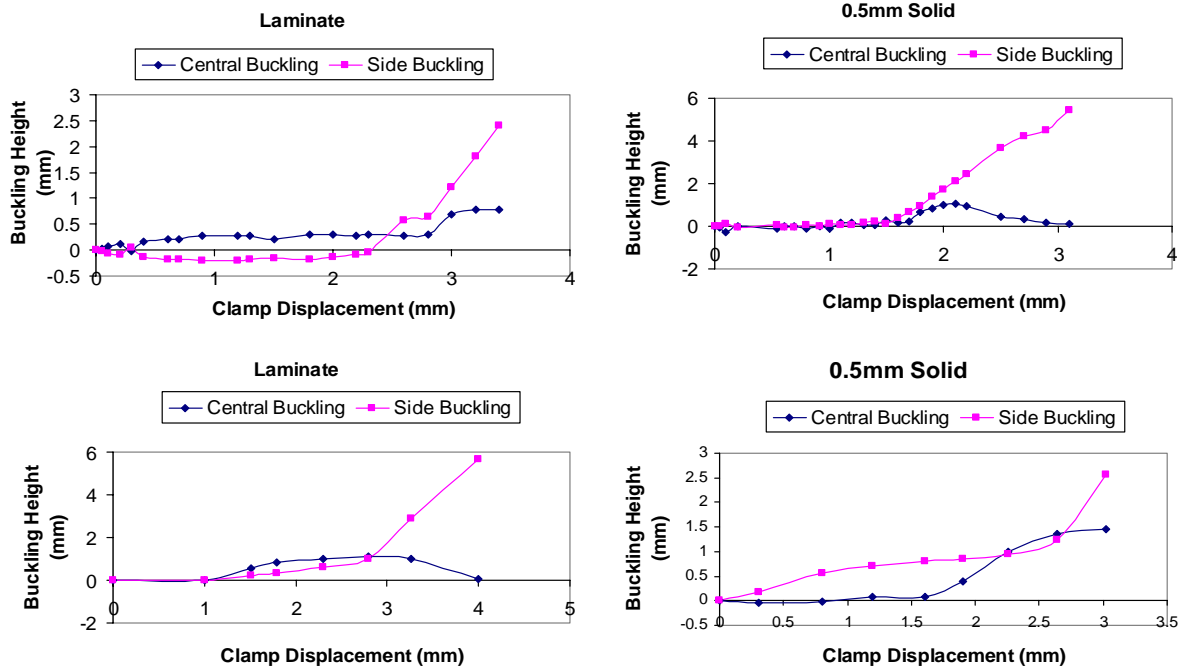


Fig. 8. The sequence of two buckling modes (B2).

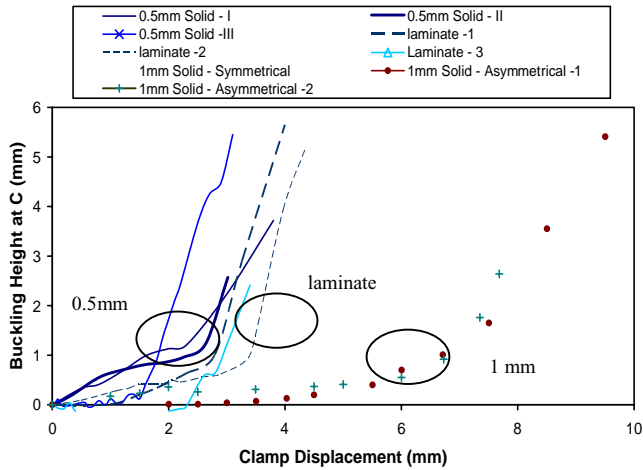


Fig. 9. Buckling height at point C (Fig. 2) vs. clamp displacement (B2).

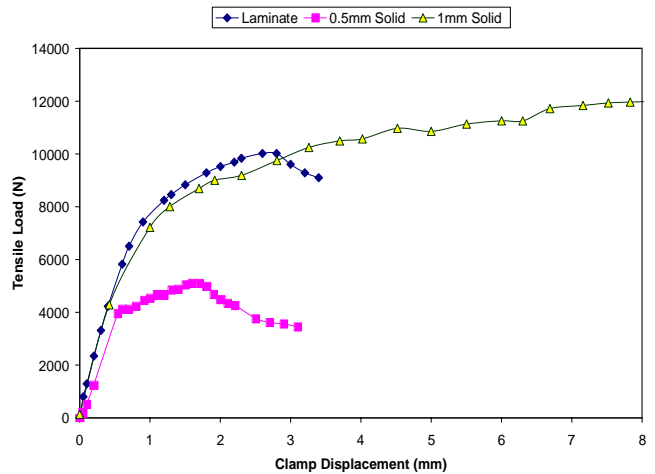


Fig. 11. Tensile load vs. clamp displacement (B2).

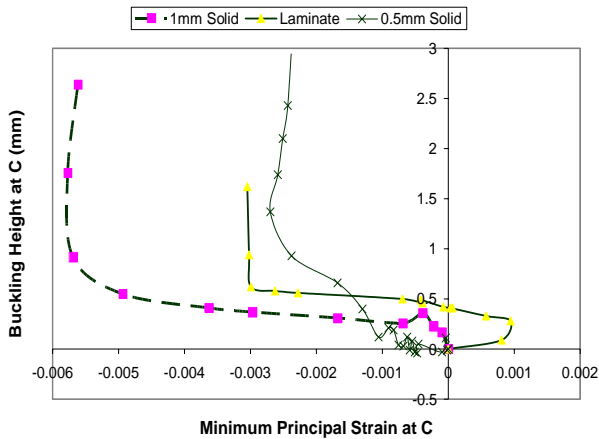


Fig. 10. Buckling height vs. local compressive strain (B2).

5 and 7 mm. The 0.5 mm laminate sheets started buckled when the clamp displacement reached 1.5~3.5 mm. When the local compressive strain is concerned, the 1 mm solid sheet shows much higher resistance to buckling, as shown in Fig. 10. Both 0.5 mm solid sheet and laminate sheet buckled at a compressive strain of 0.1%, while the 1 mm solid sheet buckled at about 0.6%. Although these strain values are still very low, however, they are much higher than the buckling strain in the B1 case.

Fig. 11 shows the plot of displacement versus tensile load. Figs. 9 and 11 together show that under boundary condition B2, the buckling initiated after the sheet deformed plastically. Plastic buckling is dominant under the B2 condition. After being removed from the fixture, the samples did not recover any noticeable amount of the buckling.

3. Yoshida buckling tests

In the Yoshida buckling test, the square metal sheet is stretched in one diagonal direction, as shown in Fig. 12. Ten-

sile deformation in the stretching direction causes a compressive stress in the transverse direction in the central region of the specimen due to the geometric constraint of the outside rigid region, and causes the wrinkle formation. The strain and deformation measurement systems are the same as used in previous wedge strip tests. Single-element strain gauges were mounted at points A and B to measure the longitudinal and transverse strains.

The tensile speed was set at 0.25 mm/min. Fig. 13 shows the 3D element deformation contour of a buckled sample.

Fig. 14 indicates that in the Yoshida buckling test, the laminate sheet has the lowest wrinkling resistance among three tested material. The 1 mm solid sheet has the highest, while the 0.5 mm sheet's resistance is slightly higher than that of the laminate sheet. The laminated sheets have relative slipping and transverse sharing, which may trigger the buckling. The buckling initiation points of 1 mm solid sheet are in the range of 2.5~3.2 mm, and the other two are in the range

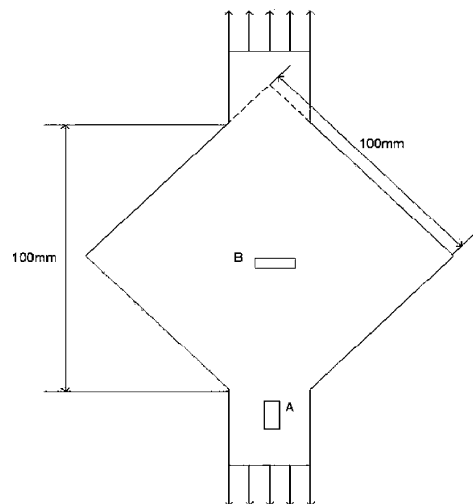


Fig. 12. The Yoshida buckling test sample.

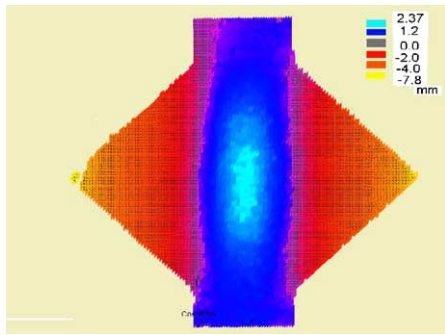


Fig. 13. Deformation contour of a Yoshida buckling test sample.

of 1–1.7 mm. When the local buckling area is concerned, the laminate sheet and the 0.5 mm solid sheet behaved similarly (Fig. 15). They both buckled at a relatively low compressive strain ($<0.3\%$), whilst the 1 mm solid sheet's critical buckling strain is a little higher at about 0.5%. Notice that the maximum span of the sample in the wedge strip test of 230 mm is almost twice the length in the Yoshida buckling test of 141 mm. Therefore, the critical buckling strain in the Yoshida buckling test is higher than that in the B1 case.

It is noteworthy that in Fig. 15, all the compressive strains were measured on the convex side. Fig. 16 is a plot of strains on both sides, from which it can be seen that for 0.5 mm and laminate sheets, the neutral surface remained as the middle surface of the solid sheet or each skin sheet, but for 1 mm sheet, the neutral surface moved out of the sheet body at the beginning. The reason could be that in order to initiate the buckling, more compressive strain was generated in the 1 mm solid sheet due to the stretching in the perpendicular direction in the pre-buckle stage than that in the other two materials.

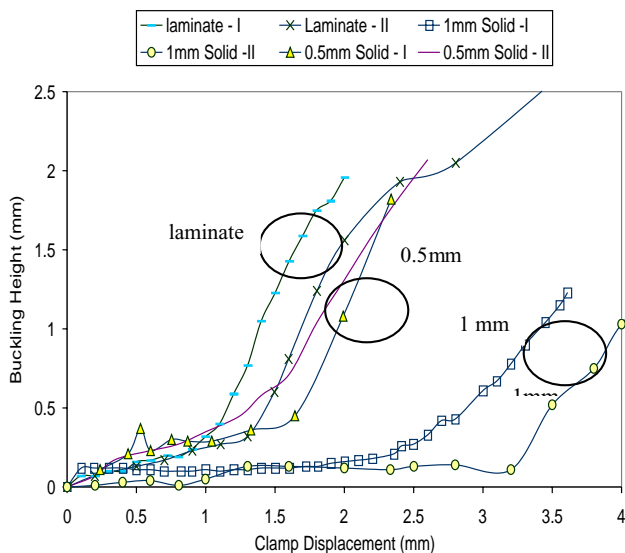


Fig. 14. Yoshida buckling test, buckling height vs. clamp displacement.

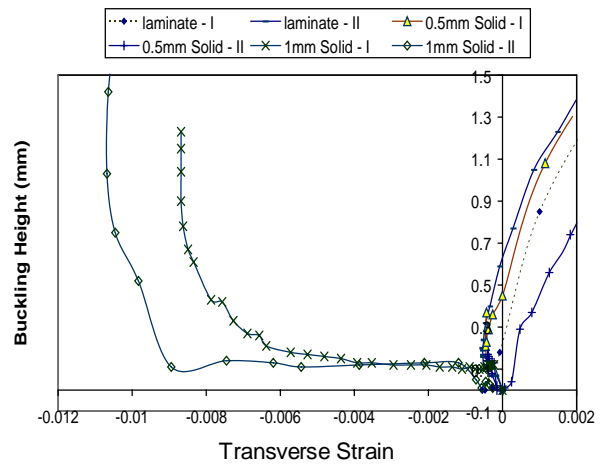


Fig. 15. Yoshida buckling test, buckling height vs. compressive strain at B.

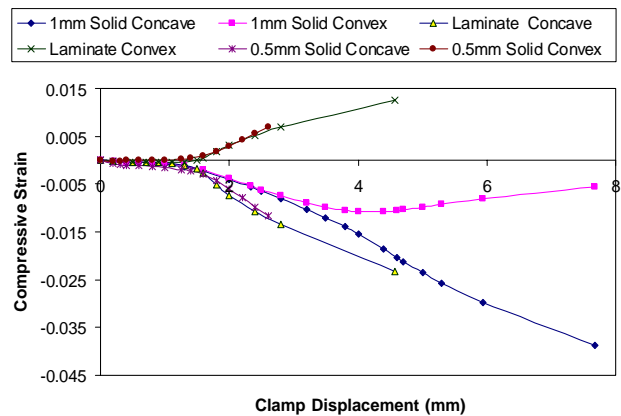


Fig. 16. Strains on the concave and convex sides.

4. Rectangular shape forming test

Rectangular shape forming tests were performed on a hydraulic press with a binder force control system. The range of the binder force is 50–500 kN and the drawing depth is 0–10 cm. The geometry of the sample is shown in solid lines in Fig. 17 and the dash lines represent the

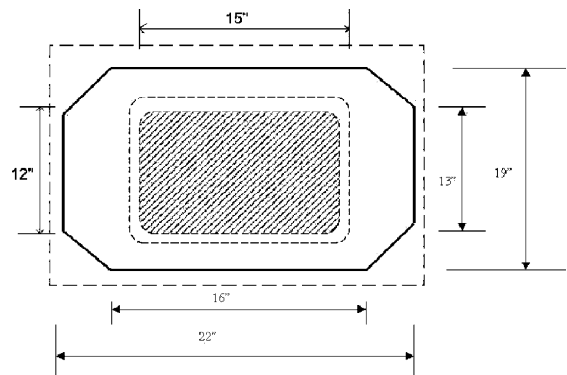


Fig. 17. Tooling and blank geometry of the forming test.

Table 3
Forming test results

Material	Draw depth (in.)	Binder force (kN)	Maximum tensile strain at the corner area (%)	Average flange wrinkling height on the side area (mm)	Side area wrinkling wave number
Laminated	2.06	320	45	1.0	15
Solid (1 mm)	2.37	332	52	0.2	15
Solid (0.5 mm)	2.25	337	64	0.3	26
Laminated	2.51	122	43	3.5	17
Solid (1 mm)	2.38	122	44	0.2	16
Solid (0.5 mm)	2.30	124	48	0.4	30
Laminated	2.30	78	34	5.1	19
Solid (1 mm)	2.38	79	39	0.4	16
Solid (0.5 mm)	2.42	79	40	3.0	30

punch (shade) and die geometry. Circle grids were etched to help in the measurement of the in-plane strains of the samples.

Fig. 18 shows a formed laminate part. Flange wrinkling occurred in all sides and the corner areas. Side-wall wrinkling was also observed in laminate parts. Table 3 is the summary of the test results, and it shows clearly that the 1 mm solid sheet has the highest wrinkling resistance. For the other two materials, the laminate sheet always had a greater buckling height than that for the 0.5 mm sheet, but this does not necessarily indicate that the laminate sheet has the lowest wrinkling resistance. It should be noticed that under the same binder force, the 0.5 mm sheet had a much higher wave number, which means that its wrinkling had been further developed than that of the other two materials. The reason 0.5 mm sheet had a relatively lower buckling height is that it could only generate a lower resistance force to counter the binder force. Thus when the wrinkling grew, it could only split into a higher-wave mode instead of increasing its height. Fig. 19 shows the pictures of the formed parts of these three materials under 80 kN binder force. The observation of wrinkling height in corner areas is shown in Fig. 20. The laminate sheet has a better performance than that of the 0.5 mm solid sheet when split failure is concerned. It split under a binder force of 448 kN and a draw depth of 6.83 cm, while the 0.5 mm solid sheet failed under 337 kN and 5.71 cm.



Fig. 18. A formed laminate part.

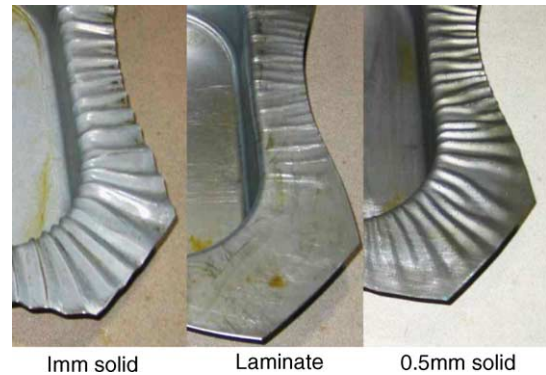


Fig. 19. Flange wrinkling under a binder force of 80 kN.

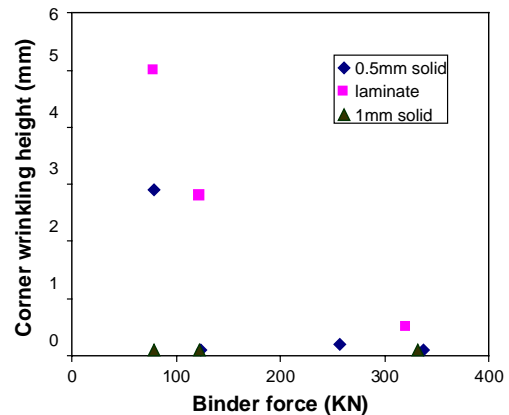


Fig. 20. Flange wrinkling height at the corner areas.

5. Conclusions

The wedge strip test, the Yoshida buckling test and the rectangular forming test have been conducted for laminated steel sheets and their skin steel sheets. Incorporation an integrating high resolution laser digitizer into the traditional Yoshida buckling test provided an efficient way to capture the deformation information. The experimental results show that it is invalid to model the laminate sheet as a solid panel, when wrinkling is concerned. This is consistent with the author's previous results [2]. All three tests showed that the

1 mm solid sheet has the highest wrinkling resistance among the three materials tested. Although the laminate sheet and the 0.5 mm solid sheet have a very similar performance, the Yoshida buckling test suggested that the laminate sheet tends to buckle slightly earlier than the 0.5 mm solid sheet, while the wedge strip test showed the opposite. Current results of the forming test cannot differentiate between the buckling resistance of the 0.5 mm solid sheet and that of the laminate sheet. Thus, step forming tests are needed in the future to study the onset and development of wrinkling for both materials.

Note that the wedge strip test here simulates side-wall wrinkling in forming, i.e. no normal constraint is applied in the sheet thickness direction. The flange wrinkling observed in the forming tests is wrinkling under constraint. Therefore, strictly speaking, two different kinds of wrinkling behavior are observed in the wedge strip test, the Yoshida buckling test and the forming test. Nevertheless, the wedge strip test is able to develop a more complex wrinkling pattern than the standard Yoshida buckling test, and hence provides a different observation of wrinkling formation and development. It has been established that the wedge strip test is a very useful tool to study the wrinkling behavior of laminate steel and other materials. Future work will further develop the test to account for normal constraints.

Acknowledgements

Support from the National Science Foundation (DMI-0115079) is gratefully acknowledged.

References

- [1] L.A. Mignery, Reduced vibration design, SAE Paper No. 951242.
- [2] H. Yao, C.C. Chen, S.D. Liu, K.P. Li, C. Du, L. Zhang, Laminated steel forming modeling techniques and experimental verifications, SAE Paper No. 2003-01-0689, 2003.
- [3] Y. Tomita, Simulations of plastic instabilities in solid mechanics. Part I, *Appl. Mech. Rev.* 47 (6) (1994) 171–205.
- [4] H. Petryk, Plastic instability: criteria and computational approaches, *Arch. Comput. Meth. Eng.* 4 (2) (1997) 111–151.
- [5] V. Tvergaard, Studies of elastic–plastic instabilities, *J. Appl. Mech.* 66 (1999) 3–9.
- [6] R. Hill, A general theory of uniqueness and stability in elastic–plastic solids, *J. Mech. Phys. Solids* 8 (1958) 236–249.
- [7] X. Wang, J. Cao, On the prediction of sidewall wrinkling in sheet metal forming processes, *Int. J. Mech. Sci.* 42 (2000) 2369–2394.
- [8] J. Cao, W.K. Liu, H.S. Cheng, H.S. Lu, A multi-scale approach for predicting wrinkling and its experimental verification, in: *Proceedings of the NSF Grantee Conference*, January 2002.
- [9] H. Lu, J.S. Chen, Adaptive meshfree particle method, *Lecture Notes Comput. Sci. Eng.* 26 (2002) 251–267.
- [10] H.S. Cheng, H.S. Lu, J. Cao, W.K. Liu, Characterization of wrinkling: experiments and simulations, in: *Proceedings of the ESAFORM Conference*, 2003.
- [11] K. Yoshida, J. Hayashi, K. Niyauchi, M. Hirata, T. Hira, S. Ujihara, Assessment of fitting behavior and shape fixation by Yoshida buckling test—a way to overall formability, in: *Proceedings of the International Symposium on New Aspects of Sheet Metal Forming ISIJ*, Tokyo, Japan, 1981, pp. 125–148.
- [12] B.W. Senior, Flange wrinkling in deep-drawing operations, *J. Mech. Phys. Solids* 4 (1956) 235–246.
- [13] T.X. Yu, W. Johnson, The buckling of annular plates in relation to the deep-drawing process, *Int. J. Mech. Sci.* 24 (1982) 175–188.
- [14] J. Cao, X. Wang, F.A. Mills, Characterization of sheet buckling phenomenon subjected to controlled boundary constraints, *ASME J. Manuf. Sci. Eng.* 124 (8) (2002) 493–501.